Scripta METALLURGICA et MATERIALIA
Vol. 27, pp. 1533-1538, 1992
Printed in the U.S.A.

CONFERENCE SET No. 1

ANNEALING TEXTURES OF BCC METALS

D.Raabe, K.Lücke,
Institut für Metallkunde und Metallphysik, RWTH Aachen, 5100 Aachen, Germany

(Received September 16, 1992)

1. Introduction

Taking up the spirit of controversy of the Zeltingen meeting and the there made comment that "the world does not only consist of aluminium", the present authors are now going to very briefly review our understanding of the development of annealing textures of bcc materials. Being studied already for 50 years, these textures were often considered to be quite similar to each other. Only in the last 10 years, mainly by applying the orientation distribution function ("ODF") f(g) [1] instead of only pole figures (g=orientation here given by the Euler angles φ_1, Φ and φ_2), the studies became thorough enough to also reveal the characteristic differences and their dependence on the various parameters. Thus, by investigating primary recrystallization induced orientation changes, the quantitative texture analysis became a powerful tool for studying the underlying recrystallization mechanisms. Also high resolution local texture measurements, e.g. by electron back scattering patterns (EBSP) in the SEM were applied [2].

In the present paper, which is based practically only on our Aachen work, the textures were determined by measuring the four incomplete polefigures {110}, {200}, {112} and {103} with $Mo_{K\alpha 1}$ radiation in the back reflection mode [3] and by deriving from them the ODFs by means of the series expansion method [1]. Such studies revealed the tendency of BCC metals to develop strong texture fibres, beside peak type components. Some important orientations and fibres are indicated in Fig.1. These make it convenient to present the ODFs in φ_1=const. sections.

2. Experimental Results

The recrystallization ("RX") textures of bcc metals can roughly be divided into three groups: group(a) those of low carbon steels (e.g. deep drawing steels), group(b) those of alloyed steels (e.g FeCr, FeSi) and group(c) those of high purity refractory metals. They strongly depend on the preceding hot rolling (HR) [4] and cold rolling (CR) textures which thus have to be briefly reviewed. For group(a), the texture of the HR band is very weak which is due to an orientation randomization by the there-occuring phase transformation (Fig.2a). The subsequent homogeneous cold rolling (Fig.2b) leads to a formation of a strong incomplete α-fibre $\{001\}<110>$-$\{111\}<110>$, accompanied by a weaker γ-fiber $\{111\}<110>$-$\{111\}<112>$.

For group(b), where no phase transformation randomizes the texture, HR yields a very inhomogeneous through thickness texture: in the center layer (Figs.3a,4a) a sharp α-fibre and close to the surface (Figs.3d,4d) strong shear components ($\{011\}<100>$ (Goss), $\{4\ 4\ 11\}<11\ 11\ 8>$, $\{110\}<112>$) due to the there-occuring strong shear deformation during HR. Here CR generally causes α-fibre formation accompanied by a weak γ-fibre in all layers (Figs.3b,3e,4b,4e). In the center layer (Figs.3b,4b) this leads to enforcing and sharpening of the α-fibre formed during HR, whereas in the surface layers (Fig.3e,4e) the shear components, especially Goss $\{011\}<100>$, rotate towards the $\{111\}<112>$ and towards the α-fibre.
For group(c), represented here by Tantalum, where also no phase transformation occurs, HR was replaced by CR with intermediate annealing (Fig.5a). The CR texture is similar to that of group(a), only the maximum is shifted along the α-fibre from $\{112\}<110>$ valied for group(a) to $\{001\}<110>$ (Fig.5b).

The annealing textures of group(a) and group(c) both reveal a strong and rather homogeneous γ-fiber with a flat maximum at $\{111\}<112>$ (Fig.2c,5c). Also for group(b) this fibre is observed for all materials and all layers, but is weaker and non-homogeneous. But there exist still certain differences between the various alloys (Figs.3c,3f,4c,4f). E.g. FeCr exposes a marked rest of the α-fibre in both layers (Figs.3c,3f), while FeSi shows a weaker α-fibre in the center and a small η-fibre $\{001\}<100>$-$\{011\}<100>$, i.e. including Goss, at the surface (Figs.4c,4f).

3. Discussion

RX occurs by the mechanisms of formation of nuclei in highly strained regions of the deformed matrix keeping the orientation of that region and by subsequent growth of the nuclei into the matrix orientation by motion of large angle grain boundaries. The texture development during RX can be discussed in terms of oriented nucleation (ON) [5], where the texture is determined by the number of growing nuclei of certain orientations, and of growth selection (GS) [6], where the texture is determined by a growth competition between differently oriented nuclei, i.e. by the mobility differences between the moving grain boundaries. Often both mechanisms will contribute to texture formation. The mechanisms of GS was shown to occur in BCC metals by Ibe and Lücke [7], by inducing random nucleation into prestrained Fe3%Si single crystals. During annealing nuclei with a $27°<110>$ orientation relationship to the deformed matrix, which is close to a $\Sigma(19a)$ coincidence, were shown to determine the final orientations (Fig.6) by winning the growth competition.

The primary recrystallization of BCC metals is characterized very generally by a nearly complete disappearance of the CR component $\{112\}<110>$ and the growth of $\{111\}<112>$. This is also to be seen for all samples presented in this paper, i.e. for all three groups (a), (b) and (c) (Figs.7 and 2 to 5). Since the orientation relationship between these two components is $35°<110>$, i.e. approximately $27°<110>$, it can be concluded that $\{112\}<110>$ is consumed by $\{111\}<112>$ due to GS. This is confirmed e.g. in microalloyed FeCr steels, where the presence of precipitations can even amplify GS. At RX temperatures above 840°C, when the coarse $(Cr,Fe)_{23}C_6$ particles are in solution, the (Ti,Nb,Fe)CN microcarbides impose a Zener drag [8] upon the boundaries. Since this drag force is proportional to the

0956-716X/92 $5.00 + .00

grain boundary energy, it can reach up to 20% of the driving force for RX in case of non-special boundaries, whereas the coincidence boundaries with their low energy are practically not hindered at all. This seems to be the reason for quite the exact 27°<110> relationship between the strong {112}<110> CR orientation and the ≈{557}<583> RX component in such steels [9]. Concerning the other RX components, only the Goss orientation experiences growth preference too: It posesses a 35°<110>, i.e. approximately 27°<110> relationship to the {111}<112> CR orientation and is observed distinctly only when this component is strongly present in the initial CR texture.

Now let us consider nucleation. The {111}<112> CR grains should easily be able to form nuclei (to grow later into {112}<110>), since they have a very fine cell structure and thus high stored energy [10]. Goss nuclei can be assumed to be formed in the shear bands of {111}<112> crystals occuring in deformed samples with high amount of soluted interstitials and large grainsize and after high deformation. In shear bands orientation changes in form of a 35°<110> // TD rotation are observed, which just lead from {111}<112> to Goss. This is also known from single crystal experiments [11]. The RX component {111}<110>, which does not exhibit a preferred growth relationship, seems to nucleate close to grain boundaries between two different adjacent {111}<112> variants [12]. In agreement with this, in the center layer of the CR textures of group(b), where {111}<112> is very weak (Figs.3b,3c,4b,4c) also the RX component {111}<110> comes out to be weaker.

The above made assumptions are largely confirmed by investigations of directionally solidified amd 90% CR iron samples which consist of only a few large grains (cm). After CR the pole figure shows two strong {111}<112> variants (Fig.8a). After annealing a sharp Goss and a minor {111}<110> component have formed (Fig.8b). In another sample of the same material a very sharp {001}<110> and a minor {111}<112> component (Fig.9a) is exposed. The annealing leads to the same {001}<110> orientation acompanied by a slight Goss (Fig.9b). The microstructure of this annealed sample (Fig.10) exposes three different regions. The left hand side which reveals a fully recovered structure without nuclei can be identified by EBSP to belong to the {001}<110> component (Fig.11a), which thus is shown to have only little tendency to form nuclei. In the middle part the coarse grained area also reveals orientations in the range of {001}<110>, (Fig.11b), but with larger scattering. On the right hand side a recrystallized zone with very small grains consists of the {111}<110> and Goss component (Fig.11c). Here obviously genuine RX took place with many nuclei being formed.

4. Conclusions

In this work three different groups (a), (b), (c) of RX textures of BCC metals are found. These are distinguished by the texture prior to cold rolling and by the elements in solution. Some important mechanisms of RX and formation of RX textures are revealed:

1.) Growth selection based on a 27°<110> orientation relationship takes place in steels and refractory metals.
2.) Finely dispersed particles strengthen the effect of growth selection.
3.) Nucleation in {111}<uvw> grains is very effective, in α-fibre grains, especially in {001}<110>, very indolent.
4.) Nucleation of Goss takes place in shear bands of {111}<112>.
5.) Oriented nucleation of {111}<110> takes place in {111}<112> grains.

5. References

1.) H.J.Bunge: Z.Metallkunde 56 (1965) 872.
2.) J.Venables, C.Harland, Phil.Mag. 27 (1973) 1193.
3.) L.G.Schulz: Journ.Appl.Phys. 20 (1949) 1030.
4.) D.Raabe, K.Lücke: Scripta Met.et Mater. 26 (1992) 1221.
5.) W.Burgers, T.Tiedema: Acta Met.1 (1953) 234.
6.) P.Beck, H.Hu: ASM Seminar on Recrystallization, Grain Growth and Textures, Met.Park, Ohio, (1966) 393.
7.) G.Ibe, K.Lücke: Archiv Eisenhüttenwesen Sept.39 (1968) 693.
8.) C.Zener: Priv.Communic. to C.S.Smith, Trans.AIME, ASM, 175 (1949) 15.
9.) D.Raabe, K.Lücke: Scripta Met.et Mater. 26 (1992) 19.
10.) I.Dillamore, P.Morris, C.Smith, W.Hutchinson: Proc.Roy.Soc. 329A (1972) 405.
11.) B.Rath, H.Hu: Trans.Met.Soc. AIME, 245 (1969) 1243.
12.) W.Hutchinson: Acta Met. 37 (1989) 1047.

6. Figures

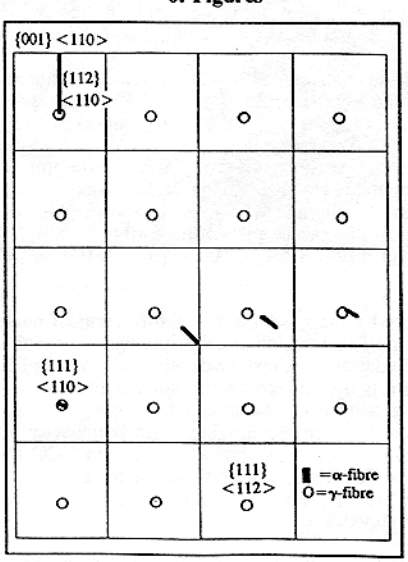

Fig.1
Some important orientations and fibres in φ_1 = const. sections.

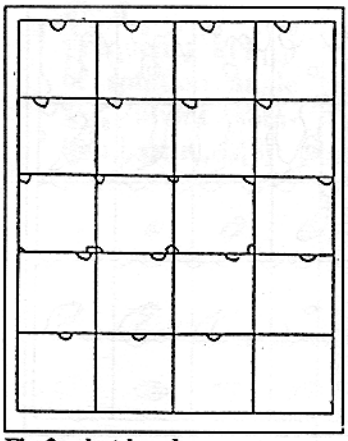

Fig.2a hot band

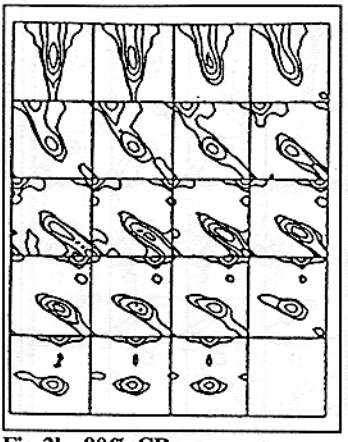

Fig.2b 90% CR

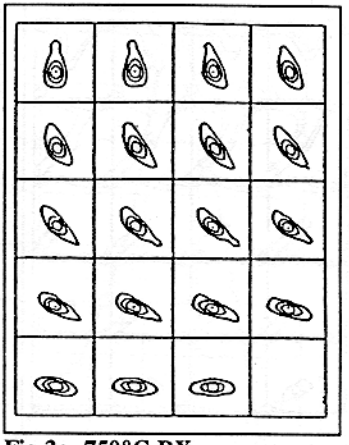

Fig.2c 750°C RX

STEEL, LOW CARBON, CENTER, φ_1=const.

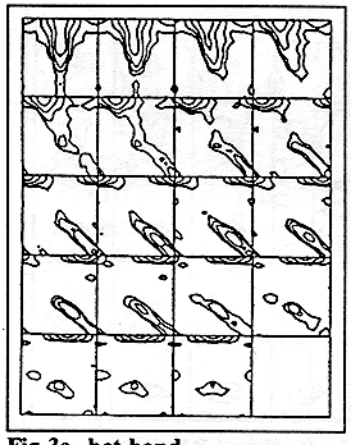

Fig.3a hot band

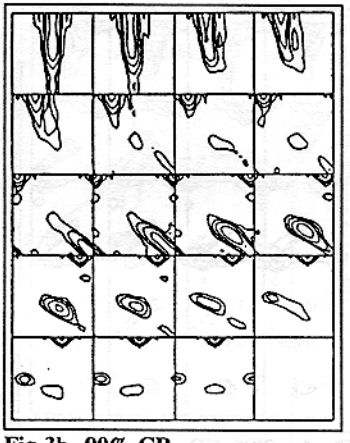

Fig.3b 90% CR

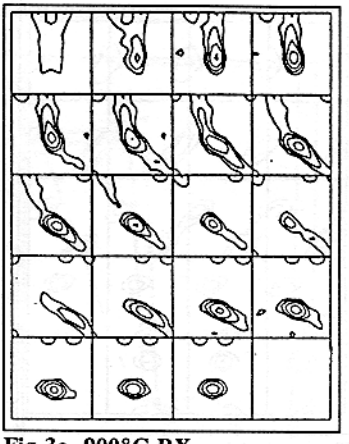

Fig.3c 900°C RX

STEEL, 17% Cr, CENTER, φ_1=const.

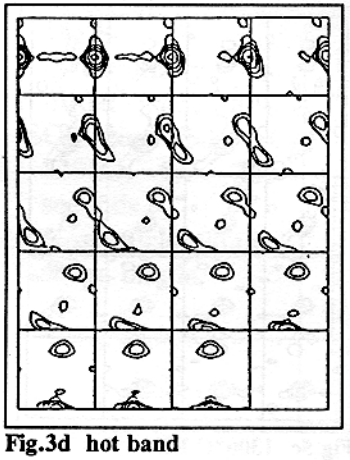

Fig.3d hot band

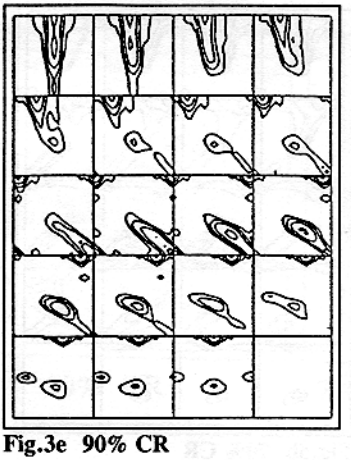

Fig.3e 90% CR

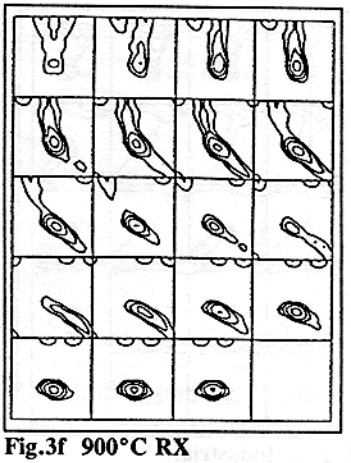

Fig.3f 900°C RX

STEEL, 17% Cr, SURFACE, φ_1=const.

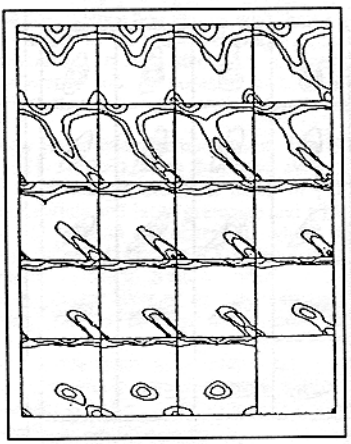

Fig.4a hot band

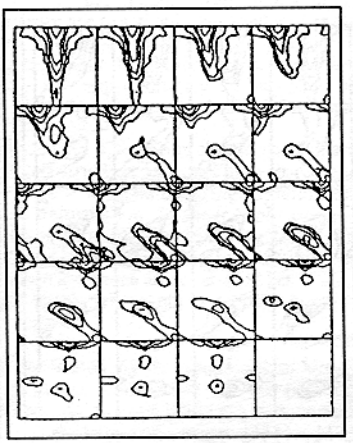

Fig.4b 90% CR

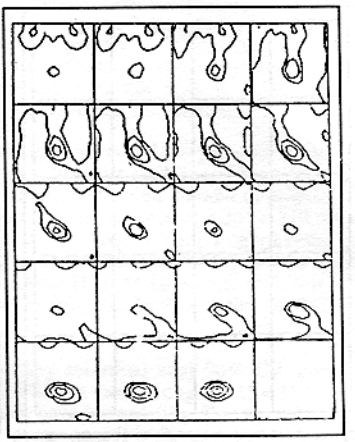

Fig.4c 800°C RX

STEEL, 3% Si, CENTER, φ_1=const.

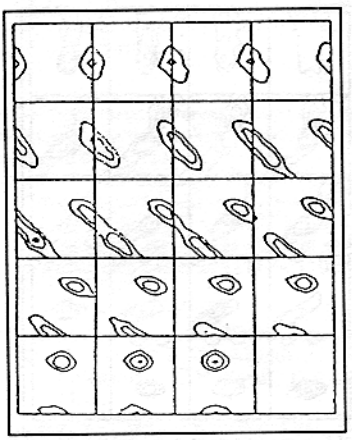

Fig.4d hot band

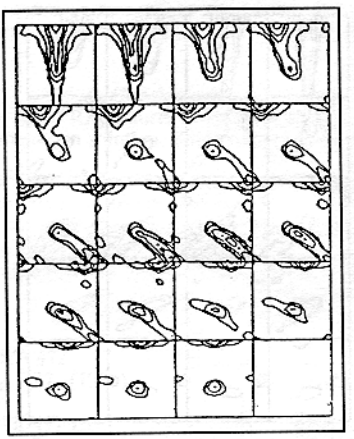

Fig.4e 90% CR

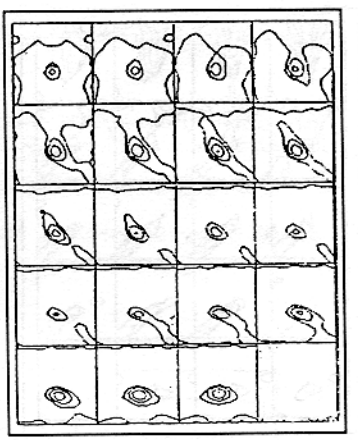

Fig.4f 800°C RX

STEEL, 3% Si, SURFACE, φ_1=const.

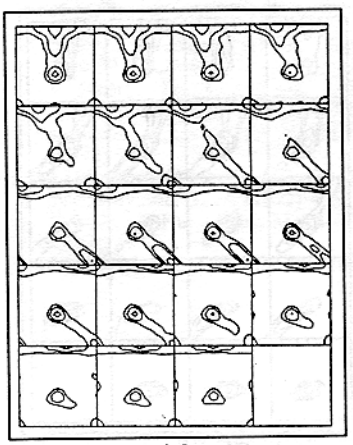

Fig.5a industrial

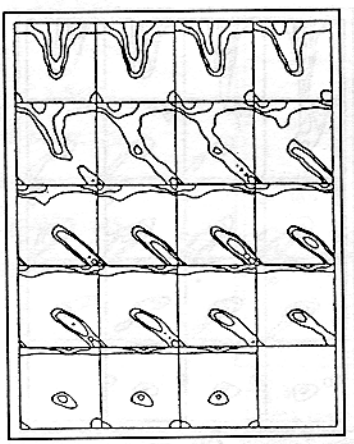

Fig.5b 70% CR

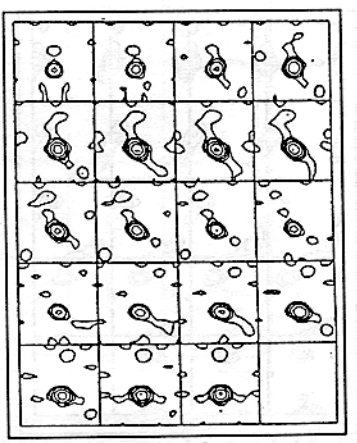

Fig.5c 1300°C RX

TANTALUM, CENTER, φ_1=const.

Fig.6
Frequency $h(\Psi_{110})$ of rotation angle Ψ_{110} about rotation axis r_{110}. [8]

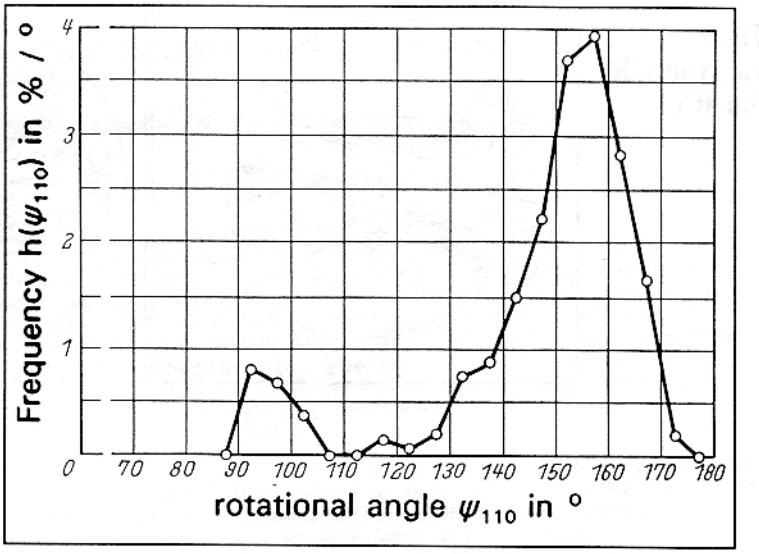

Fig.7
increase of {111}-<112> and decrease of {112}-<110> during annealing. Three different dispersion rates of cementite.

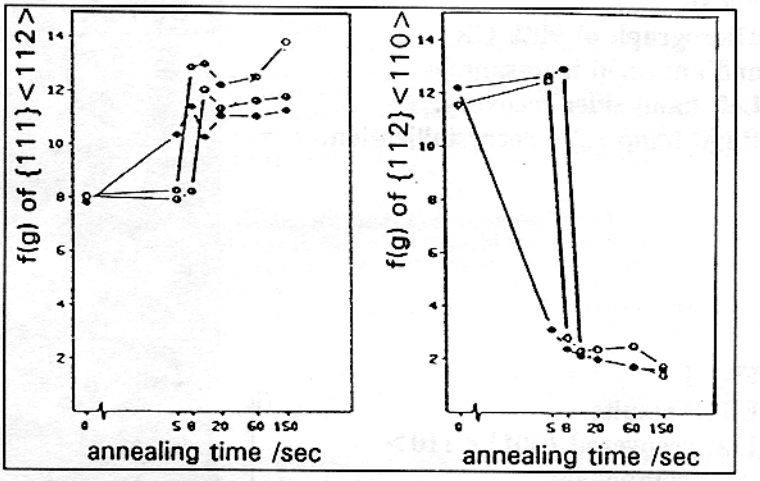

Fig.8
directionally solidified iron. 90% CR and RX at 720°C for 300 seconds.
Goss nucleation in shear bands.

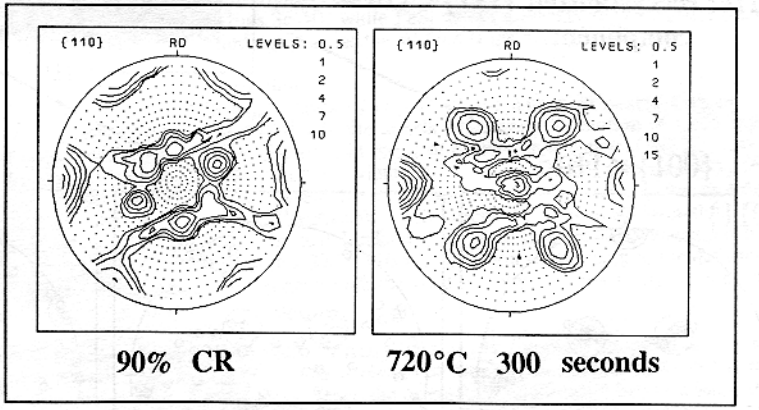

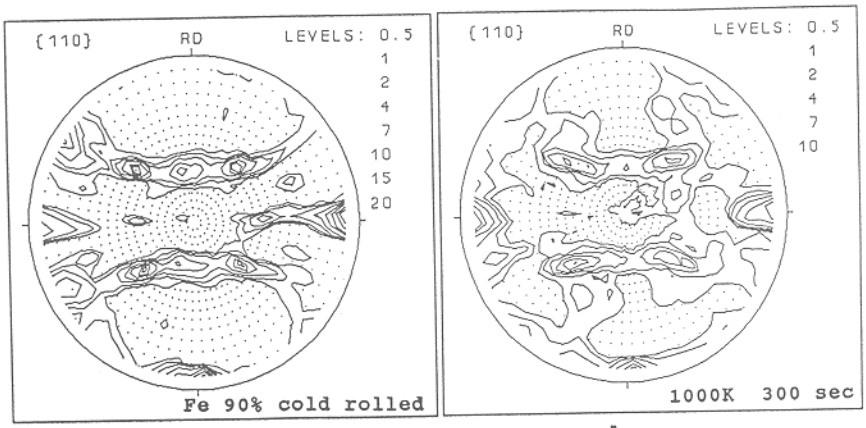

Fig.9
9a: iron CR
9b: RX

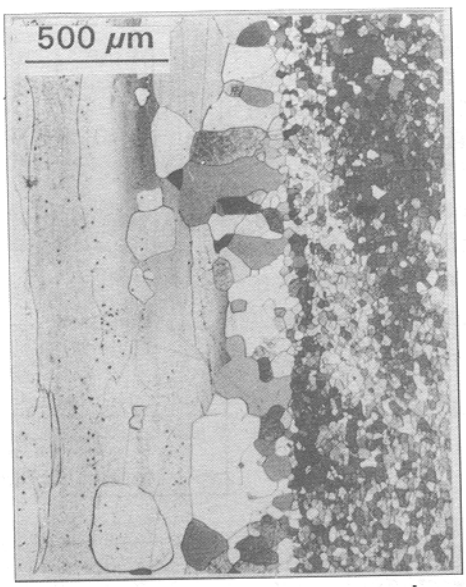

Fig.10
Micrograph of 90% CR and annealed iron sample.
Left hand side: recovery.
Right hand side: recrystallization.

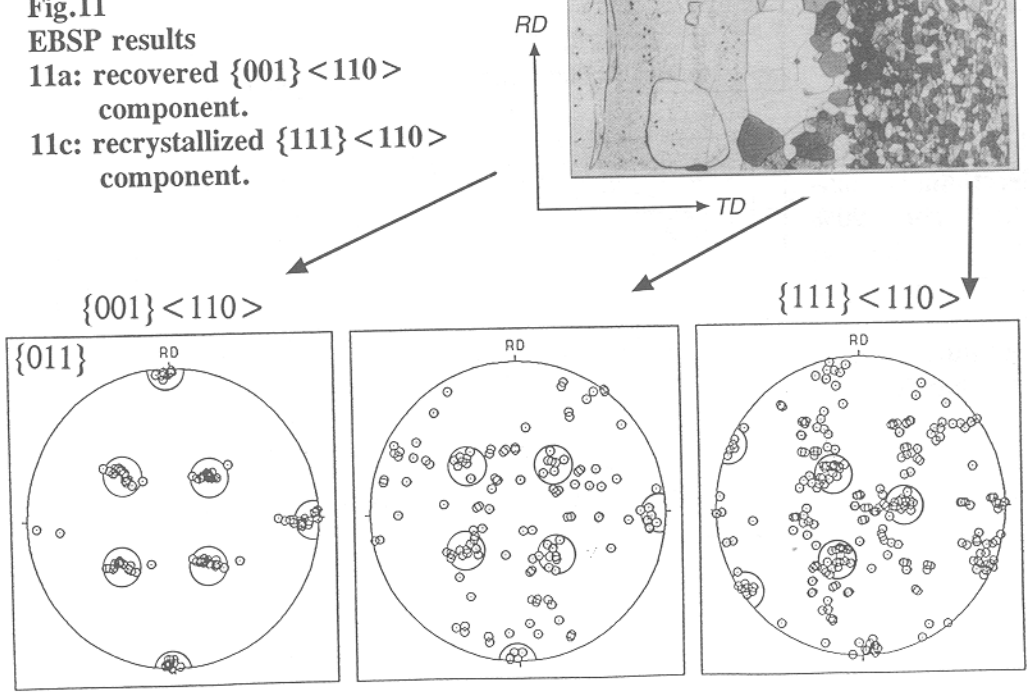

Fig.11
EBSP results
11a: recovered {001}<110> component.
11c: recrystallized {111}<110> component.